Real-time deformability cytometry: on-the-fly cell mechanical phenotyping

Oliver Otto[1], Philipp Rosendahl[1], Alexander Mietke[1], Stefan Golfier[1], Christoph Herold[1], Daniel Klaue[1], Salvatore Girardo[1], Stefano Pagliara[2], Andrew Ekpenyong[1,3], Angela Jacobi[1], Manja Wobus[4], Nicole Töpfner[5], Ulrich F Keyser[2], Jörg Mansfeld[1], Elisabeth Fischer-Friedrich[6,7] & Jochen Guck[1,2]

We introduce real-time deformability cytometry (RT-DC) for continuous cell mechanical characterization of large populations (>100,000 cells) with analysis rates greater than 100 cells/s. RT-DC is sensitive to cytoskeletal alterations and can distinguish cell-cycle phases, track stem cell differentiation into distinct lineages and identify cell populations in whole blood by their mechanical fingerprints. This technique adds a new marker-free dimension to flow cytometry with diverse applications in biology, biotechnology and medicine.

Mechanical phenotyping has long been discussed as a marker-free way of quantifying functional changes of physiological and pathological origin in cells[1]. This idea has been validated in the context of cell differentiation[2–4] and malignant transformation[5–7] and has spawned the development of many basic research methods[8]. These techniques generally have throughput rates of 10–100 cells/h, which is far too low for applications in biology, biotechnology and medicine, for which a throughput comparable to that of standard flow cytometers is required.

One important hydrodynamic approach starting to address this need is deformability cytometry (DC)[9], in which cells are deformed by deceleration at the stagnation point of fast extensional flow. The ensuing deformation is imaged for a few seconds with a high-speed camera at 100,000 frames/s (f.p.s.). Owing to the massive amount of data generated, the analysis has to be performed off-line, and results are available only after ~15 min. Using DC, Tse *et al.* were able to demonstrate the translational utility of mechanical phenotyping for the diagnostic analysis of pleural effusions[7]. DC enables measurement rates of ~1,000 cells/s, comparable to that of fluorescence-based flow cytometers, but the total number of cells analyzed is limited to a few thousand.

Here we introduce RT-DC, in which on-the-fly analysis of deformed cell shape enables continuous measurement and the total number of cells analyzed is, in principle, unlimited. In contrast to DC—in which cells are deformed by inertial forces—with RT-DC, cells are flowed through a microfluidic channel constriction and deformed without contact by shear stresses and pressure gradients (**Fig. 1**). This aspect is similar to previous studies of red blood cell (RBC) deformability in microfluidic channels[10–12]. RBCs are relatively soft and can be deformed at low flow velocities. However, the analysis of shear stress–induced deformation for stiffer cells has not been demonstrated as it requires higher stresses, and thus higher velocities, which introduce considerable technical and methodical demands. RT-DC achieves this by the following innovations in experimental design, data acquisition and analysis.

The deformed cell inside the constriction is illuminated with a pulsed, high-power LED and imaged with a complementary metal-oxide semiconductor (CMOS) camera at 2,000–4,000 f.p.s. (**Fig. 1a** and Online Methods). The camera-triggered LED light pulses are 1 µs in duration—short enough to prevent motion blurring of the cells, which flow with ~10 cm/s and deform from a spherical into a bullet-like shape (**Fig. 1b**). CMOS cameras have been used before for the fast imaging of RBC deformations[13], but the images acquired were analyzed off-line only. Here we applied an image analysis algorithm (Online Methods), executed on a standard personal computer, that continuously acquires images from the camera in real time, detects the presence of a cell, determines its contour (**Supplementary Fig. 1a**), quantifies its deformation (D = 1 − circularity) and size (cross-sectional area) and displays the results in a scatter plot (**Fig. 1c** and Online Methods). This feat enables the continuous analysis of cell deformation in real time with measurement rates of several hundreds of cells per second (see **Supplementary Video 1**) and >100,000 cells (for RBCs as well as other cell types) analyzed in a single experimental run.

The cell deformation D inside the constriction is not independent of cell size, as larger cells experience greater stresses and deform more. We have developed a hydrodynamic model (Online Methods) that calculates the tangential (shear) and normal stresses (pressure) over a spherical cell's surface (**Fig. 1d**) and can be used to derive the expected deformations of an isotropic, linearly elastic sphere (**Supplementary Fig. 1b**). The resulting shapes for Young's moduli on the order of 1 kPa resemble those of the bullet-shaped cells in the experiment. This analytical modeling, not feasible for methods relying on inertial forces, effectively decouples size and deformation, and it permits the introduction of isoelasticity lines as additional parameterization of the scatter plots (**Fig. 1e**) and the extraction of material properties.

[1]Biotechnology Center, Technische Universität Dresden, Dresden, Germany. [2]Cavendish Laboratory, University of Cambridge, Cambridge, UK. [3]Department of Physics, Creighton University, Omaha, Nebraska, USA. [4]Medizinische Klinik 1, Universitätsklinikum Carl Gustav Carus, Technische Universität Dresden, Dresden, Germany. [5]Klinik und Poliklinik für Kinder und Jugendmedizin, Universitätsklinikum Carl Gustav Carus, Technische Universität Dresden, Dresden, Germany. [6]Max Planck Institute for the Physics of Complex Systems, Dresden, Germany. [7]Max Planck Institute of Molecular Cell Biology and Genetics, Dresden, Germany. Correspondence should be addressed to J.G. (jochen.guck@tu-dresden.de).

RECEIVED 30 JULY 2014; ACCEPTED 23 DECEMBER 2014; PUBLISHED ONLINE 2 FEBRUARY 2015; DOI:10.1038/NMETH.3281

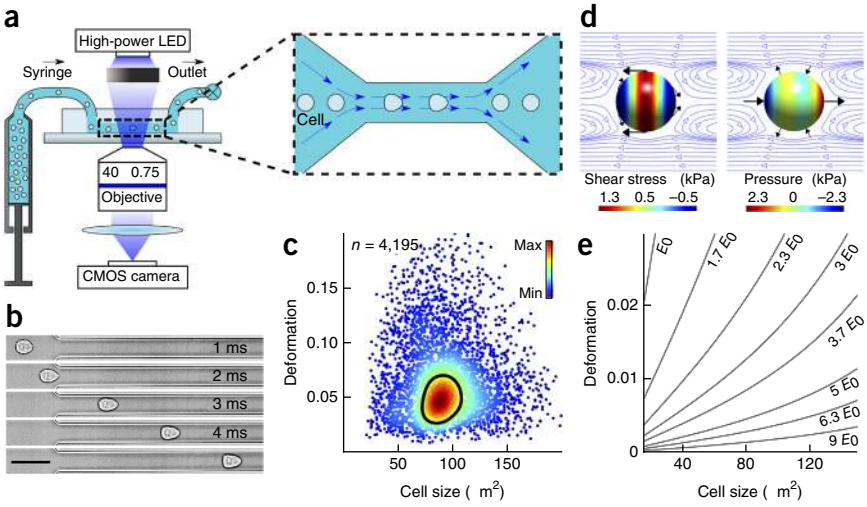

Figure 1 | Real-time deformability cytometry (RT-DC). (**a**) Setup and measurement principle (inset shows top view of constriction). (**b**) Time series of a cell deformed through constriction. Scale bar, 50 µm. (**c**) Scatter plot of deformation versus cell size (cross-sectional area) of 4,195 cells (dots) obtained in 45 s. Color indicates a linear density scale; black line, 50%-density contour. No cells were smaller than 20 µm². (**d**) Shear stress (left) and pressure (right) on the cell surface inside the constriction. Black arrows indicate stress directions; surface color indicates magnitude; blue lines show the flow profile in a co-moving reference frame. (**e**) Isoelasticity lines divide the size-deformation scatter plots into areas of identical stiffness for multiples of a given elastic modulus E_0.

As a first demonstration of the utility of RT-DC, we obtained dose-response curves of cytoskeletal drugs on cell deformability (Online Methods and **Supplementary Fig. 2**). Deformation of HL60 cells increased with increasing concentrations of cytochalasin D, a drug effectively disassembling filamentous actin (**Fig. 2a** and **Supplementary Fig. 3**). Although sensitivity to drugs affecting intermediate filaments has been reported for a variant of DC[14], the actin sensitivity (and microtubule sensitivity; data not shown) connects RT-DC to cytoskeletal research on the progression through the cell cycle[15–18]. Thus, we tested whether RT-DC can distinguish cells chemically synchronized in different cell-cycle stages. Characteristic changes in size, deformation and overlap with isoelasticity bands were seen (**Fig. 2b**). The ability to distinguish G2- from M-phase cells, at least in part caused by changes in the actin cytoskeleton (**Supplementary Fig. 4b–d**), is notable because this discrimination has not been demonstrated with DC and is impossible with FACS. Because cell size—assessed by forward scattering—remains approximately the same, and the amount of DNA—measured using propidium iodide (PI), BrdU (5-bromodeoxyuridine) or EdU (5-ethynyldeoxyuridine) fluorescence—is identical, G2 and M cells cannot be resolved by FACS (**Fig. 2c**). In contrast, the overlap of G2 and M phase decreases considerably in RT-DC–measured deformation distributions, and distinction becomes possible (**Fig. 2d**). Thus, RT-DC is ideally suited for applications in which the analysis of cell-cycle progression and cell proliferation in living cells and without external labels is desired.

Another physiological process that has been implicated in stiffness changes is the differentiation of cells. We differentiated HL60 cells into granulocytes, monocytes and macrophages and compared their mechanical fingerprints using RT-DC (**Fig. 3a**). Granulocytes and monocytes were more deformable than undifferentiated HL60 cells, whereas macrophages were stiffer—a finding consistent with previous optical stretcher results[4]. We further differentiated primary human hematopoietic stem cells (HSCs; CD34⁺ cells) from bone marrow (BM-CD34⁺) *in vitro* into the same three mature myeloid cell types, which showed the same mechanical difference between granulocytes/monocytes and macrophages (**Fig. 3b**), a distinction not easily made with FACS (**Supplementary Fig. 5c**). Comparing HL60 cells directly to primary HSCs showed considerable differences in size and deformation (**Fig. 3c**). This was expected because HL60 cells are immortal and differ from their primary counterparts in several aspects, and even mechanical differences have been previously seen by optical stretching[4]. Particularly interesting is the difference between CD34⁺ cells from bone marrow (BM-CD34⁺) and peripheral blood (PB-CD34⁺) despite their being identified by the same molecular surface marker. PB-CD34⁺ cells constitute a rather homogeneous population mobilized into the peripheral blood after administration of recombinant granulocyte

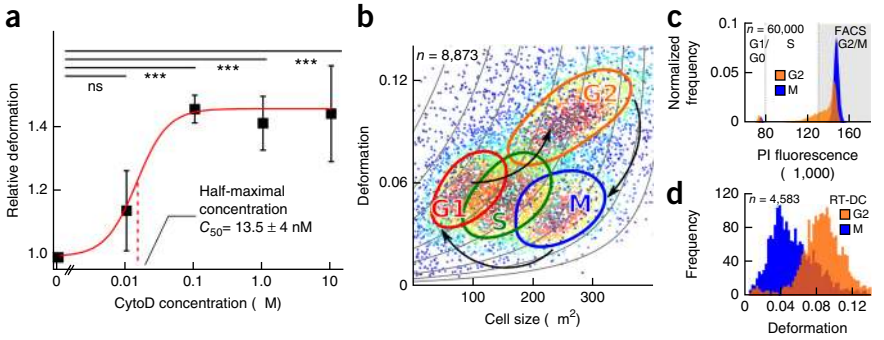

Figure 2 | Sensitivity to cytoskeletal drugs and cell-cycle progression. (**a**) Dose-response curve showing the increasing HL60 cell deformation relative to untreated controls as a function of cytochalasin D (cytoD) concentration. Data points show the mean of three independent repeats ± s.e.m. Statistical significance is determined by bootstrapping the deformation sample distributions and a subsequent paired *t*-test for each concentration; ***$P < 0.001$; ns, not significant. Red line, sigmoidal saturation fit. (**b**) 50%-density contour plots and measurement data of HL60 cells chemically synchronized in G1, S, G2 and M phases of the cell cycle, measured in separate experiments but shown in one plot (see **Supplementary Fig. 4a**). Black arrows indicate progression through the cell cycle. (**c**) FACS plots of DNA amount (propidium iodide (PI) fluorescence, in relative units) of cells in G2 and M phases. 67% and 92% of all detection events, respectively, fall into the same G2/M gating area (gray background). (**d**) Distributions of RT-DC deformation of G2- and M-phase cells with much smaller overlap than with FACS in **c**. All RT-DC measurements were carried out in a 20 µm × 20 µm channel.

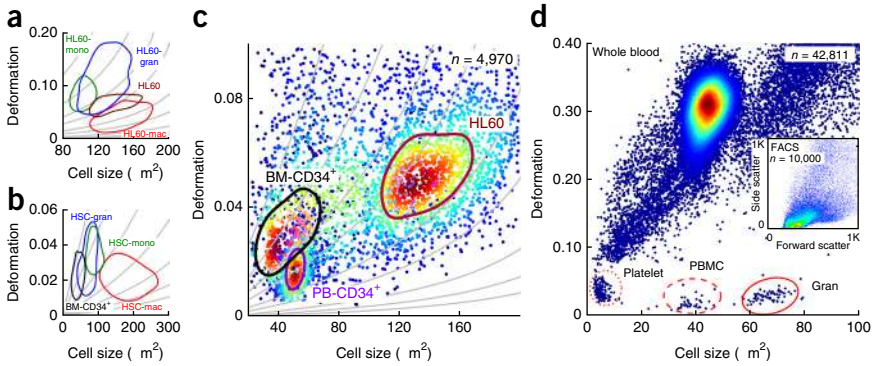

Figure 3 | Mechanical phenotyping of blood cells and their precursors. (**a**) 50%-density contour plots of HL60 cells differentiated into granulocytes (HL60-gran), monocytes (HL60-mono) or macrophages (HL60-mac) (20 µm × 20 µm channel, 0.04 µl/s flow rate; see **Supplementary Fig. 5a**). (**b**) 50%-density contour plots of hematopoietic stem cells (HSCs) from bone marrow (BM-CD34$^+$) differentiated into the same cell types as in **a** (30 µm × 30 µm channel, 0.16 µl/s flow rate; see **Supplementary Fig. 5b**). (**c**) RT-DC scatter plots of HL60 cells, primary HSCs from peripheral blood (PB-CD34$^+$) and BM-CD34$^+$ cells measured in separate experiments at a flow rate of 0.04 µl/s in a 20 µm × 20 µm channel, shown in one plot. Also shown are 50%-density contour lines. (**d**) RT-DC scatter plot of whole blood (diluted 1:50 in PBS containing 0.5% methylcellulose) measured at a flow rate of 0.04 µl/s in a 20 µm × 20 µm channel. Apart from the large fraction of red blood cells at large deformation, three distinct subpopulations are visible and circled with red dotted (platelets), dashed (peripheral blood mononucleated cells, PBMC) and solid lines (granulocytes, gran). Inset shows forward (size) and side scattering (granularity) in a FACS plot of the same sample with no distinct populations visible.

colony–stimulating factor (G-CSF). In contrast, BM-CD34$^+$ cells are more heterogeneous, containing cells in G2 and M phases and from a continuous spectrum of differentiation, which are absent in PB-CD34$^+$ cells. This difference is not detectable with FACS based on size or CD34$^+$ expression levels.

Arguably the biggest appeal of mechanical phenotyping lies in the label-free identification of different, and especially less frequent, cells in a mixed population; for example, the cell types present in whole blood. Here the real-time analysis, enabling continuous measurement, becomes essential. It allowed us to assess ~40,000 blood cells in 85 s (**Fig. 3d**). The very abundant RBCs were clearly separated from the other cells by their greater deformation, revealing at least three additional cell populations. This shift of the RBCs away from the other blood cell types is a distinct advantage of RT-DC over label-free FACS analysis (**Fig. 3d** and **Supplementary Fig. 6**). Separate analysis identified the remaining populations as platelets, peripheral blood mononucleated cells and granulocytes (**Supplementary Fig. 7a–d**). The stimulation of granulocytes with phorbol 12-myristate 13-acetate (PMA) resulted in a clear change in their mechanical fingerprint (**Supplementary Fig. 7e**), which, together with the small interdonor variability (**Supplementary Fig. 7f,g**), points to future diagnostic applications of RT-DC.

Cytomechanical analysis of human blood could become a functional correlate to the blood smear routinely performed in human medicine. It would add a dynamic dimension of cell function to the currently static analysis of cell morphology. Future addition of multiwavelength fluorescence analysis is straightforward and will enable cross-correlation of mechanics with standard cytological markers used in FACS. Real-time analysis also opens the possibility for active sorting based on mechanical properties and fluorescence in Bayesian combination, setting RT-DC apart from passive mechanical sorting approaches in which sorting is fixed by microfluidic channel geometry and optimized for a particular deformability, size and flow speed[19,20]. RT-DC has the potential to find widespread application in diverse fields of biology, biotechnology and medicine, where a label-free characterization of cell function is a desired and so far unmet need.

METHODS

Methods and any associated references are available in the online version of the paper.

Note: Any Supplementary Information and Source Data files are available in the online version of the paper.

ACKNOWLEDGMENTS

We thank A. Taubenberger, M. Herbig, C. Liebers, L. Menschner, C. Klug, R. Berner, M. Bornhäuser, C. Bryant, E. Chilvers, B. Friedrich, A. Voigt, J. Tegenfeldt, M. Tschöp, F. Amblard, T. Hyman and S. Grill for technical support, advice and engaging discussions. The HL60/S4 cells were a generous gift of D. and A. Olins (University of New England). Financial support from the Alexander-von-Humboldt Stiftung (Humboldt-Professorship to J.G.), Sächsisches Ministerium für Wissenschaft und Kunst (TG70 grant to O.O. and J.G.), DFG-Center for Regenerative Medicine of the Technische Universität Dresden (seed grant to J.G.), Deutsche Forschungsgemeinschaft (DFG Emmy Noether Grant to J.M., MA 5831/1-1; KFO249 Gerok position to N.T.), Deutsche Gesellschaft für Pädiatrische Infektiologie (N.T.) and Studienstiftung des Deutschen Volkes (A.M.), Max Planck Society (E.F.-F.) and Leverhulme and Newton Trust (Early Career Fellowship to S.P.) is gratefully acknowledged.

AUTHOR CONTRIBUTIONS

J.G. conceived of the method; O.O. and J.G. designed most experiments and wrote the manuscript; O.O. and P.R. wrote the real-time analysis software; P.R. built the pulsed LED illumination and designed the lithography masters; O.O., P.R., D.K. and C.H. optimized the imaging; S. Girardo, S.P. and U.F.K. provided technical advice and help with soft lithography; A.M., O.O. and E.F.-F. developed the analytical model; S. Golfier performed and analyzed the cytoskeletal drug experiments; J.M. designed and interpreted the cell-cycle synchronization experiments; P.R. performed and analyzed the cell-cycle experiments; A.E. cultured and differentiated the HL60 cells; A.J. and M.W. designed the HSC separation and differentiation experiments; A.J. performed the HSC separation and differentiation; A.J. and O.O. measured and analyzed the HL60 and HSC cells; N.T., C.H. and O.O. performed and analyzed the whole blood and separated blood cell measurements.

COMPETING FINANCIAL INTERESTS

The authors declare competing financial interests: details are available in the online version of the paper.

1. Elson, E.L. *Annu. Rev. Biophys. Biophys. Chem.* **17**, 397–430 (1988).
2. Titushkin, I. & Cho, M. *Biophys. J.* **93**, 3693–3702 (2007).
3. Lautenschläger, F. *et al. Proc. Natl. Acad. Sci. USA* **106**, 15696–15701 (2009).
4. Ekpenyong, A.E. *et al. PLoS ONE* **7**, e45237 (2012).
5. Remmerbach, T.W. *et al. Cancer Res.* **69**, 1728–1732 (2009).
6. Kumar, S. & Weaver, V.M. *Cancer Metastasis Rev.* **28**, 113–127 (2009).
7. Tse, H.T. *et al. Sci. Transl. Med.* **5**, 212ra163 (2013).
8. Van Vliet, K.J., Bao, G. & Suresh, S. *Acta Mater.* **51**, 5881–5905 (2003).
9. Gossett, D.R. *et al. Proc. Natl. Acad. Sci. USA* **109**, 7630–7635 (2012).
10. Skalak, R. & Branemark, P.I. *Science* **164**, 717–719 (1969).

11. Noguchi, H. & Gompper, G. *Proc. Natl. Acad. Sci. USA* **102**, 14159–14164 (2005).
12. Wan, J., Ristenpart, W.D. & Stone, H.A. *Proc. Natl. Acad. Sci. USA* **105**, 16432–16437 (2008).
13. Sawetzki, T., Eggleton, C.D., Desai, S.A. & Marr, D.W.M. *Biophys. J.* **105**, 2281–2288 (2013).
14. Dudani, J.S., Gossett, D.R., Tse, H.T. & Di Carlo, D. *Lab Chip* **13**, 3728–3734 (2013).
15. Matthews, H.K. *et al. Dev. Cell* **23**, 371–383 (2012).
16. Kunda, P. & Baum, B. *Trends Cell Biol.* **19**, 174–179 (2009).
17. Kline-Smith, S.L. & Walczak, C.E. *Mol. Cell* **15**, 317–327 (2004).
18. Stewart, M.P. *et al. Nature* **469**, 226–230 (2011).
19. Hur, S.C., Henderson-MacLennan, N.K., McCabe, E.R.B. & Di Carlo, D. *Lab Chip* **11**, 912–920 (2011).
20. Beech, J.P., Holm, S.H., Adolfsson, K. & Tegenfeldt, J.O. *Lab Chip* **12**, 1048–1051 (2012).

ONLINE METHODS

RT-DC setup. The experimental setup for real-time and high-throughput mechanical cell analysis (**Fig. 1**) consists of the following features. The microfluidic chip is made of poly(dimethylsiloxane) (PDMS; Sylgard 184, VWR) using standard soft-lithography methods. After cross-linking the polymer for 45 min at 70 °C and opening inlet and outlet with a 1.5-mm biopsy puncher (Harris Unicore, Sigma-Aldrich), the bottom of the chip is sealed with a glass cover slide (Thickness 2, Hecht) after plasma surface activation (PDC 32-G, Harrick) of the PDMS. The microfluidic chip has two reservoirs connected by a 300-µm-long narrow channel (constriction) with a 20 µm × 20 µm or 30 µm × 30 µm square cross-section depending on maximum cell size. Cell size should be between 50% and 90% of the channel size so that shear gradients are large. Clogging by cell clumps and debris occurs in about 10% of the chips; this could be further reduced by introduction of a row of filter posts.

After fabrication, the chip is assembled on the *xy* stage of an Axiovert 200M inverted microscope (Zeiss) and connected to a syringe pump (NemeSyS, Cetoni) for driving a cell suspension through the channel (**Fig. 1a** inset). In all experiments a flow rate between 0.02 µl/s and 0.2 µl/s is applied. A sheath flow geometry centers the cells laterally, and lift forces center them vertically within the channel, so that they are always in focus. For a given flow rate and channel cross-section, the velocity of a cell depends on its size. The velocity vs. cell-size distribution is measured experimentally and can be described theoretically (see analytical model below). For a flow rate of 0.04 µl/s and a cell diameter of 15 µm, the final cell velocity inside a 20 µm × 20 µm channel is approximately 15 cm/s.

In order to reduce motion blurring of cells during translocation through the constriction, a high-power LED (CBT-120, 462 nm, Luminus Devices) is operated with a pulsed current for sample illumination. Pulses are triggered by the camera shutter to ensure synchronized image exposure. When the LED is operated at a pulse duration of 1 µs and a cell velocity of 15 cm/s, motion blurring is reduced to about 0.15 µm. This is sufficient to reliably characterize the deformation of cells.

Images of deformed cells are acquired using a CMOS camera (MC1362, Mikrotron), which is connected to a standard PC via full camera link interface (NI-1433 Frame Grabber, National Instruments). At full resolution this camera can operate at more than 500 frames per second (f.p.s.). For a reduced region of interest (ROI), acquisition rates of up to 100,000 f.p.s. can be achieved. In the experiments described, the camera is typically run at 4,000 f.p.s. with an ROI of 250 × 80 pixels. All image processing steps are carried out using a standard six-core PC. At the moment, the algorithm is capable of performing image acquisition, image analysis and data storage for several hundred cells per second in real time. In practice, the ability for real-time analysis is limited only by the number of cells available.

In compliance with *Nature Methods*' material-sharing policy, the setup is available for running reasonable and limited, non-commercial trial experiments at the Biotechnology Center of the Technische Universität Dresden, Dresden, Germany, at the user's expense and subject to signing a license agreement.

Image analysis. The image processing algorithm is implemented in a C++/LabVIEW environment. Although LabVIEW (LabVIEW 2012, National Instruments) is used as a user interface, all time-critical calculations are carried out as C++ code using the OpenCV computer vision library (http://opencv.org) compiled into dynamic link libraries running on three dedicated CPU cores. Communication between different threads is achieved by queues. In the current implementation of the software the complete processing time of a single frame is less than 250 µs.

In practice, the first core acquires a single frame from the camera. The image is assigned a unique handle ID and transferred to a second core responsible for image preprocessing. These tasks include background subtraction and thresholding to create a binary image. Next, on a third core, the presence of a cell in the image is detected, and the contour of the cell, if present, is determined using a border-following algorithm[21]. From the contour the algorithm derives the cell cross-sectional area, perimeter and position and calculates the circularity *c*, which is the main quantity used to characterize the deformation of cells. Here the circularity is defined as

$$c = \frac{2\sqrt{\pi A}}{l}$$

where A is the projected cell surface area and l is its perimeter. Obviously, for an ideal circle, $c = 1$; and for any deformation, $c < 1$. The deformation of a cell is defined as $D = 1 - c$, as this quantity increases with deformation away from a round shape. Because the measurement output is a text file of shape information, and there is no need to save images or videos, the typical data size of an experiment with 10,000 cells measured is on the order of 1 MB.

Analytical model. The analytical model developed in this work allows the calculation of the flow profile around a spherical object moving in a cylindrical microfluidic channel. It derives the hydrodynamic stresses on the object surface and quantifies its deformation on the basis of linear-elasticity theory. Applying this analytical model to RT-DC data, the relationship between cell size–dependent stress, deformation and elastic material parameters is disentangled (A.M., O.O., S. Girardo, P.R., A. Taubenberger, *et al.*; unpublished data). The main steps are outlined below.

RT-DC operates at Reynolds numbers below 0.1, which allows neglecting the inertial terms in the Navier-Stokes equation. The hydrodynamic stresses applied with the RT-DC setup are calculated in two steps. First, a closed solution to the Stokes equation for a sphere advected in a cylindrical channel[22] is employed to extract steady-state flow profiles, velocities of the sphere and sphere size–dependent surface stresses. In the second step, the concept of the equivalent channel radius[23] is used to map the results to the square cross-section geometry in the RT-DC setup. The force acting on the sphere is characterized by two counteracting contributions (**Fig. 1d**): a net force due to the normal pressure distribution over the sphere, which acts mostly in the direction of the flow ($F_p > 0$) and pushes and pulls at the rear and front side of the cell, respectively; and a net viscous shear force from the shear stresses acting particularly at cell surface regions that are closest to the channel walls, which holds the cell back ($F_s < 0$). Although cells are moving without net force in steady state ($F_p + F_s = 0$), the anisotropy of the surface stresses leads to the observed bullet-like deformations (**Supplementary Fig. 1**). Values of peak shear and

normal stresses, and hence deformations, depend on the cell size relative to the channel dimensions.

To disentangle the relation between cell size–dependent hydrodynamic stress and resulting deformations, we employ an analytical model that calculates deformations of an elastic sphere under the hydrodynamic load present in the RT-DC setup. Briefly, we use an analytical solution for the equilibrium equation of an isotropic, incompressible, linearly elastic medium, which contains free constants that have to be adapted to appropriate boundary conditions[24]. The form of this general deformation solution and the hydrodynamic stress permit the derivation of the resulting deformations analytically by using the latter as boundary conditions for the deformation problem. In the deformation vs. area scatterplot representation, a cell population that varies only in size but is homogeneous in its elastic properties would cover a path that is approximated by isoelasticity lines derived from the analytical model (**Fig. 1e**). Calculation of those isoelasticity lines is done by fixing the elastic modulus in the model and increasing the sphere radius while leaving all experimental parameters constant. Eventually area and deformation are derived from the resulting theoretical shapes. The model is also capable of extracting elastic parameters by shape-fitting of the experimentally observed cell shapes (A.M., O.O., S. Girardo, P.R., A. Taubenberger, *et al.*, unpublished data).

Note that the observed cross-sectional area of a deformed cell is not necessarily equal to the cross-sectional area of the nondeformed cell. Hence, it is possible that two cells with identical elastic moduli but different cell volumes have very similar cross-sectional areas in their deformed state but differ in the measured deformation. According to our model, this effect is particularly prominent for the case of large deformations where isoelasticity lines become increasingly steep in size-deformation plots (see **Fig. 2b**).

To apply comparable stresses in microfluidic channels of different dimensions (for example, side length L and L' of two different cross-sectional channel areas), the flow rate has to be changed by a factor of $(L'/L)^3$, which follows from simple scaling arguments.

RT-DC measurement procedure. Cells in suspension are centrifuged at 115*g* for 5 min (5805 R, Eppendorf) and resuspended in a solution of phosphate saline buffer without Mg^{2+} and Ca^{2+} (PBS–) and 0.5% (w/v) methylcellulose (Sigma-Aldrich) to a final concentration of 10^6 cells/ml. Usually an absolute sample volume of 100 µl is sufficient for RT-DC studies. Addition of methylcellulose increases the density of the buffer and helps to reduce sedimentation of the cells during the experiment. Methylcellulose also increases the viscosity of the medium and thus allows higher shear forces at lower flow velocities. It has been shown that methylcellulose can be used as a component of cell culture media[25] without biological alterations to the cells[26].

The cell suspension is kept at 37 °C before being drawn into a 1-ml syringe. The syringe is connected to the chip by polymer tubing, which is extensively cleaned by flushing with ethanol (70%) and 200 nm–sterile-filtered (Millipore, Sigma-Aldrich) deionized water. After sample loading and connecting the tubing to the inlet and outlet of the chip, the flow is usually stabilized for 2 min at a constant flow rate before starting the measurement. All data acquisition is carried out at the rear part of the 300-µm-long constriction where the cell shape has reached steady state. In a typical experiment, between 1,000 and 100,000 cells are analyzed, depending on the sample concentration and the requirements of the particular experiment, at three different flow rates. After each condition the flow is stabilized for 2 min. As a reference, the circularity of the nondeformed cells in the reservoir is confirmed for all experiments (see **Supplementary Fig. 8** for three typical examples).

Cells. *HL60 cells.* Most of the experiments were done on HL60 cells, a myeloid precursor cell line, which has served as a standard suspended cell line in comparable experiments with an optical stretcher[4]. Where appropriate, results were confirmed with primary cells. The HL60 cell line was originally derived from a patient suffering from APL in 1977 and modified to the current HL60/S4 line (a generous gift from D. and A. Olins of the Department of Pharmaceutical Sciences, College of Pharmacy, University of New England, who had confirmed the cell line before sending) used in this work[27]. Cells were cultured in RPMI-1640 medium (Life Technologies) with 10% FCS (Life Technologies) and 1% penicillin/streptomycin (Life Technologies) in a standard incubator (Hera Cell, Thermo Scientific) at 37 °C, 5% CO_2 and 95% air. The cells were split every 48 h and resuspended to a concentration of 2×10^5 cells/ml. For experiments, cells were taken during log phase, approximately 36 h after splitting. Cells were initially checked for mycoplasma contamination (Mycoplasma Kit, Sigma-Aldrich) and regularly renewed from frozen stocks.

HL60-gran, HL60-mono and HL60-mac. As a myeloid precursor cell line, *in vitro* differentiation of HL60 cells into granulocyte-like, monocyte-like and macrophage-like cells can be induced, which have many properties resembling those of primary cells. The differentiation protocol is as follows[4]. Briefly, for generating HL60-derived granulocytes (HL60-gran) all-*trans*–retinoic acid (Sigma-Aldrich) with a final concentration of 1 µM was added to a T-25 cell culture flask. The concentration of cells was kept at 1.5×10^5 cells/ml. HL60-derived monocytes (HL60-mono) were obtained using 1-α, 25 dihydroxyvitamin D3 (Sigma-Aldrich) at 100 nM while cell concentration was kept constant at 1.5×10^5 cells/ml. HL60-derived macrophage (HL60-mac) differentiation was induced with phorbol 12-myristate 13-acetate (PMA; Sigma-Aldrich) at 16 nM. Cell density was adjusted to 2.5×10^5 cells/ml. Successful differentiation required 96 h for neutrophils and monocytes and 24 h for macrophages and was tested by proliferation as well as fluorescence assays[4].

HSCs. $CD34^+$ human hematopoietic stem cells (HSCs) were obtained from granulocyte colony–stimulating factor (G-CSF)-mobilized peripheral blood (PB-$CD34^+$) or from bone marrow (BM-$CD34^+$) of healthy donors. With informed consent, following the Institutional Review Board-approved protocols EK221102004 and EK263122004, we selected $CD34^+$ cells from apheresis or bone marrow products by immunomagnetic selection using CD34 progenitor-cell isolation MicroBeads (Miltenyi), following the instructions of the manufacturer. The purity of the $CD34^+$ population after selection was determined to be >97% using FACS. All FACS measurements in this study were done with an LSR II flow cytometer (BD Bioscience).

HSC-gran, HSC-mono and HSC-mac. In vitro differentiation and expansion of primary HSCs was carried out for bone marrow–derived $CD34^+$ cells over 21 d. For granulocyte differentiation[28], BM-$CD34^+$ cells were seeded in serum-free Cellgro medium

doi:10.1038/nmeth.3281

(CellGenix) and cultured for 21 d in the presence of the following cytokines. For the first 4 d, the medium contained recombinant human G-CSF (30 ng/ml), GM-CSF (5 ng/ml) (PeproTech), SCF (50 ng/ml), FLT3L (100 ng/ml) and IL-3 (5 ng/ml) (Miltenyi). At days 4, 7, 11, 14, 17 and 21, cells were harvested, washed and either expanded (day 4: IL-3 and G-CSF; days 7–21: G-CSF) or directly used for analysis. For monocyte and macrophage differentiation, G-CSF was substituted by GM-CSF and M-CSF (30 ng/ml), respectively[29]. The surface expression of the stem cell marker CD34 and of lineage-specific markers (granulocytes CD15 and CD66b; monocytes and macrophages CD14 and CD11b) was quantified after 21 d by FACS (data not shown).

Primary blood cells. The blood samples of healthy volunteers were drawn with a 20-gauge Multifly needle into an S-Monovette (either 9 ml EDTA or 10 ml sodium citrate) by vacuum aspiration (Sarstedt). The study was approved by the Institutional Review Board of the University Medical Center Carl Gustav Carus at the Technische Universität Dresden (EK89032013). Written informed consent was obtained from all participants before any study procedure. For whole blood measurements, the drawn blood was diluted 1:50 in PBS– containing 0.5% (w/v) methylcellulose. For erythrocyte depletion (**Supplementary Fig. 7a**), 2.5 ml Dextran 6% (w/v) (Dextran 500, Pharmacosmos) were added to 10 ml of whole blood and mixed by inverting four times. After sedimentation of erythrocytes, the supernatant was centrifuged for 10 min at 260*g* and cells were gently resuspended in PBS– containing 0.5% (w/v) methylcellulose for RT-DC measurements. From a second blood sample of the same donor, granulocytes, PBMCs and erythrocytes (**Supplementary Fig. 7b–d**) were highly purified by a two-gradient density centrifugation with 42% and 51% Percoll (GE Healthcare Biosciences). Granulocyte activation was induced by 60 ng PMA per 10^6 cells and an incubation for 30 min at 37 °C (**Supplementary Fig. 7e**). RT-DC measurements of primary blood cells were performed in channels with a cross-section of 20 µm × 20 µm at a flow rate of 0.04 µl/s.

Viability tests. For all cells used in this study, the viability after RT-DC measurement was tested. For HL60 cells, a discrimination between apoptotic and necrotic cells was performed by an annexin V–FITC/PI FACS assay following a standard protocol (Life Technologies), which assesses phosphatidylserine (PS) translocation together with membrane integrity. Control cells were taken from the same cell culture flask and treated the same way except for not carrying out the RT-DC measurement. FACS analysis revealed a cell viability post-RT-DC of 94% ± 1% compared to 97% ± 1% of the controls (see **Supplementary Fig. 9**). To study long-term effects, we monitored the rate of growth of post-RT-DC HL60 cells for 5 d and compared it to the growth of controls. Trypan blue (Sigma-Aldrich) staining was carried out 6, 24, 48, 72, 96 and 120 h after the experiment, and the number of viable cells was counted using a Neubauer chamber, revealing no significant differences in viability between post-RT-DC cells (97%) and controls (98%). The viability of peripheral blood– and bone marrow–derived $CD34^+$ cells was continuously monitored to over 95%, analyzed with Trypan blue and annexin V/PI using microscopy and FACS, following the instructions of the manufacturer (Miltenyi).

Drug treatments. To test the sensitivity of RT-DC to alterations in the cytoskeleton, we treated HL60 cells with different concentrations of cytochalasin D (cytoD; Sigma-Aldrich). CytoD is an inhibitor of actin polymerization and leads to a destabilization of the cell actin cortex. Prior to the experiment, cells were resuspended in PBS– and 0.5% (w/v) methylcellulose as described above and incubated with the respective concentration of cytoD for 10 min at 37 °C. This study was performed using 0.01 µM, 0.1 µM, 1 µM and 10 µM cytoD dissolved in 0.0025%, 0.025%, 0.25% and 2.5% (v/v) dimethyl sulfoxide (DMSO), respectively. As DMSO (Sigma-Aldrich) was used as a solvent, its effect on cell deformation was verified using RT-DC applying the same protocol. Up to a concentration of 1% (v/v) DMSO, no significant change in relative deformation was observed (**Supplementary Fig. 2c** inset).

Statistical significance was determined by bootstrapping the deformation sample distributions and subsequent conduction of a paired *t*-test[30] for each concentration of cytoD. Here, the mean of the bootstrapping distribution for every drug treatment was tested against the null hypothesis that relative deformation equals unity. The effect of cytoD on HL60 cells for a given concentration is declared significant from the experimental repetition with the highest *P* value. The effect of cytoD concentration on relative deformation is described by fitting a sigmoidal dose-dependence model to the data, which allows for calculation of a unified median (half-maximal) dose C_{50}.

Cell-cycle synchronization. HL60 cells were presynchronized at the border of G1/S by a standard double-thymidine block and release protocol. In brief, cells were treated for 20 h with thymidine (2.5 mM, Sigma-Aldrich) followed by a release (two washing steps, each consisting of centrifugation at 180*g* for 5 min and resuspension in PBS–) into fresh medium for 9 h and a second 16-h thymidine block. This procedure yields a highly synchronized population of HL60 cells with a fraction of more than 90% in G1/S as measured by cell-cycle analysis with a standard flow cytometer as described below. For S phase, presynchronized cells were released for 30 min. G2 cells were then additionally incubated with 9 µM CDK1 inhibitor RO3306 (VWR) for further 5 h. Mitotic cells were obtained by releasing presynchronized cells into fresh medium containing 10 µM dimethylenastron (DMA; VWR) for 10 h. DMA is an analog of monastrol preventing centrosome separation, which results in monopolar spindle formation and a subsequent mitotic checkpoint–dependent arrest[31]. G1-phase cells were produced by releasing cells after a double-thymidine block into clean medium. After 12 h, more than 90% had undergone mitosis and were in G1 as confirmed by flow cytometry measurements. Samples synchronized in G1, S, G2 and mitosis were characterized in the RT-DC setup following the protocol described above.

In parallel, the synchronized samples were fixed and stained for cell-cycle analysis using standard flow cytometry. Fixation was done with ice-cold absolute ethanol yielding a final concentration of 80% (v/v). The fixed cells were washed and incubated for 40 min in a PBS– solution containing 5 µg/ml PI (Sigma-Aldrich), 10 µg/ml RNase A (Life Technologies) and 0.05% (v/v) Triton X-100 (G-Bioscience).

Fluorescence imaging and staining. Confocal images of cytoD-treated and cell-cycle phase–synchronized cells (**Supplementary Figs. 3** and **4b**) were obtained with an upright confocal laser

scanning microscope (LSM 700, Zeiss). Cells were kept in suspension at a concentration of about 10^6 cells/ml and fixed in 4% paraformaldehyde (Sigma-Aldrich), incubated for 20 min and then washed with PBS–. Subsequently, 50 µl of cell suspension were placed on a Superfrost Plus gold microscope slide (Gerhard Menzel GmbH), whose surface binds sedimented cells. After permeabilization with 0.2% Triton X-100 (G-Bioscience) for 5 min, the adhered cells were carefully rinsed four times using PBS–. This washing procedure was applied after each step of the protocol. Cells were then incubated in 50 µl of a staining solution containing 2.8 µM 4′,6-diamidino-2-phenylindole (DAPI; Life Technologies) and 0.4 µM phalloidin tetramethylrhodamine (TRITC; Sigma-Aldrich) in PBS– for 1 h in the dark. One drop of ProLong antifade (Life Technologies) was added, and the cells were sealed with a coverslip.

21. Suzuki, S. & Abe, K. *Comput. Vis. Graph. Image Process.* **30**, 32–46 (1985).
22. Haberman, W.L. & Sayre, R.M. Motion of rigid and fluid spheres in stationary and moving liquids inside cylindrical tubes (Research and Development Report 1143) (Hydromechanics Laboratory, Department of the Navy, 1958).
23. Huebscher, R.G. *ASHVE Trans.* **54**, 101–118 (1948).
24. Lurie, A.I. *Theory of Elasticity* (Springer, 2005).
25. Ogawa, M., Parmley, R.T., Bank, H.L. & Spicer, S.S. *Blood* **48**, 407–417 (1976).
26. Goldblum, S., Bae, Y.K., Hink, W.F. & Chalmers, J. *Biotechnol. Prog.* **6**, 383–390 (1990).
27. Leung, M.F., Sokoloski, J.A. & Sartorelli, A.C. *Cancer Res.* **52**, 949–954 (1992).
28. Kiani, A. *et al. Exp. Hematol.* **35**, 757–770 (2007).
29. Ginhoux, F. & Jung, S. *Nat. Rev. Immunol.* **14**, 392–404 (2014).
30. Maloney, J.M. & Van Vliet, K.J. *Soft Matter* **10**, 8031–8042 (2014).
31. Mayer, T.U. *et al. Science* **286**, 971–974 (1999).

doi:10.1038/nmeth.3281